

# Dopant-Induced Symmetry Breaking Reveals Hidden Magnons in a Spin-Orbit Correlated Material

Dirk Wulferding,<sup>1</sup> Francesco Gabriele,<sup>2</sup> Wojciech Brzezicki,<sup>3,4</sup> Mario Cuoco,<sup>2</sup> Changyoung Kim,<sup>5,6</sup> Mariateresa Lettieri,<sup>2</sup> Anita Guarino,<sup>2</sup> Antonio Vecchione,<sup>2</sup> Rosalba Fittipaldi,<sup>2</sup> and Filomena Forte<sup>2</sup>

<sup>1</sup>*Department of Physics and Astronomy, Sejong University, Seoul 05006, Republic of Korea*

<sup>2</sup>*CNR-SPIN, c/o Università di Salerno, IT-84084 Fisciano (SA), Italy*

<sup>3</sup>*Institute of Theoretical Physics, Jagiellonian University,  
ulica S. Łojasiewicza 11, PL-30348 Kraków, Poland*

<sup>4</sup>*International Research Centre MagTop, Institute of Physics,  
Polish Academy of Sciences, Aleja Lotników 32/46, PL*

<sup>5</sup>*Center for Correlated Electron Systems, Institute for Basic Science, Seoul 08826, Republic of Korea*

<sup>6</sup>*Department of Physics and Astronomy, Seoul National University, Seoul 08826, Republic of Korea*

Correlated materials with competing spin-orbit and crystal-field interactions can host composite spin-orbital magnons that are highly susceptible to structural and electronic perturbations, enabling control of magnetic dynamics beyond spin-only physics. Using Raman spectroscopy on  $\text{Ca}_2\text{RuO}_4$ , we show that the partial substitution of Ru by Mn reconstructs the magnon spectrum and leads to one-magnon modes that are hidden in the undoped state. We demonstrate that the transition-metal substitution activates otherwise symmetry-forbidden magnon modes through mirror-symmetry breaking of the underlying spin-orbital configuration. This effect can be theoretically explained by the local structural distortions induced in the  $\text{RuO}_6$  octahedra near the dopant, that enable the observation of mixed-parity one-magnon modes. The uncovered mechanism demonstrates how spin-orbit-lattice entanglement can be exploited to control collective magnetic excitations in spin-orbit correlated materials.

Spin-orbit coupling (SOC) in correlated electron systems can fundamentally reshape magnetic ground states and excitations, giving rise to phenomena that go beyond conventional spin-only descriptions. When SOC, crystal-field splittings, and electron correlations are of comparable magnitude, spin, orbital, and lattice degrees of freedom become strongly entangled, enabling unconventional forms of magnetism and collective excitations [1–5]. Understanding how these intertwined interactions respond to controlled perturbations is a central challenge in the study of quantum materials.

$\text{Ca}_2\text{RuO}_4$  is a prototypical spin-orbit-coupled Mott insulator that exhibits anomalous ground-state responses and a rich phase diagram [6–12] arising from the interplay of spin, orbital, and lattice degrees of freedom,[11, 13–17] with still debated properties particularly about the metal-insulator transition under nonequilibrium conditions [18–26]. Below the metal-insulator transition, the distortions of the  $\text{RuO}_6$  octahedra become more pronounced, and an antiferromagnetic insulating phase emerges with a Néel temperature  $T_N \approx 110$  K [9, 27–29]. While initially described in terms of localized  $S = 1$  moments of  $\text{Ru}^{4+}$  ( $4d^4$ ), it is now understood that the magnetism of  $\text{Ca}_2\text{RuO}_4$  arises from a competition between SOC and crystal-field effects, leading to a spin-orbital-entangled ground state [14, 16, 30–33].  $\text{Ca}_2\text{RuO}_4$  is then placed in proximity of a  $d^4$  excitonic magnetism, in which long-range order emerges from the coupling of spin-orbit excitons rather than from preformed local moments [34–37].

Magnetic excitations in  $\text{Ca}_2\text{RuO}_4$  reflect this entanglement, exhibiting strong anisotropy, sizable excitation

gaps, and modes with mixed spin-orbital character, as revealed by neutron scattering, Raman and resonant inelastic scattering spectroscopies [14, 16]. A challenging feature of this material is the sensitivity of its magnetic properties to lattice distortions. Changes induced by temperature, pressure, strain, or chemical substitution can reconstruct the magnetic ground state [31, 38–44]. This pronounced spin-orbital-lattice coupling makes  $\text{Ca}_2\text{RuO}_4$  an ideal platform for exploring how symmetry breaking and structural perturbations can be exploited to tune collective magnetic dynamics in spin-orbit-coupled materials. Indeed, exploring how these composite excitations are expected to get reconstructed under controlled perturbations, such as chemical doping or strain, opens a pathway to engineering magnetic excitations through spin-orbit-lattice entanglement, a frontier that promises novel mechanisms for quantum control in correlated oxides. In the context of chemical doping it has been realized that the substitution of the transition metal element in correlated oxides can be a powerful way to control the coupled spin-orbital-lattice dynamics [45, 46]. This approach goes beyond conventional charge or bandwidth control, and represents an alternative route to tailor the spin-orbital interactions through orbital-moment dilution [45, 46].

Observability of collective magnetic excitations is governed by crystal symmetry and experimental selection rules. As a consequence, a portion of the magnon spectrum may remain hidden, being symmetry-forbidden. Optical and neutron-scattering studies have revealed that structural perturbations, reduced dimensionality, or hybridization with lattice degrees of freedom can ren-

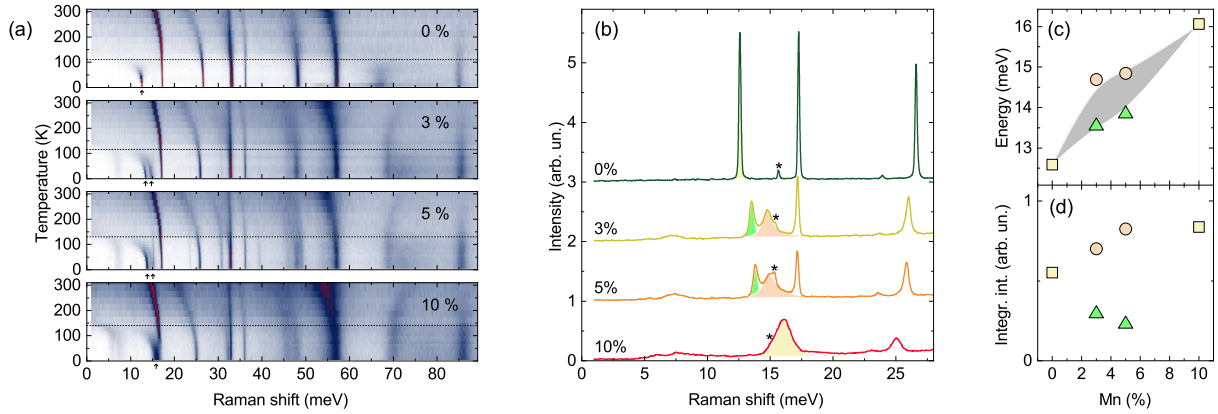


FIG. 1. (a) Temperature-dependent Raman spectra of  $\text{Ca}_2(\text{Ru},\text{Mn})\text{O}_4$  with 0%, 3%, 5%, and 10% Mn content measured in the  $B_{1g}$  symmetry channel. Dashed lines mark the Néel temperatures. The arrows indicate one-magnon excitations. (b) Individual Raman spectra measured at  $T = 4$  K. One-magnon contributions are shaded. The black asterisks mark a phonon that partially overlaps with magnons. (c) Magnon energies and (d) their integrated intensities as a function of Mn content.

der otherwise forbidden one-magnon modes observable [47, 48]. Hybrid magnon-phonon excitations [49] and nonreciprocal magnons [50] further illustrate how subtle symmetry breaking [51–53] can dramatically reshape magnetic excitation spectra. Despite these advances, controlled pathways to activate hidden magnons in bulk spin-orbit correlated materials, without inducing a global structural phase transition remain scarce. Addressing this gap is crucial to establishing spin-orbital-lattice engineering as a viable route for controlling collective magnetic excitations in correlated materials.

In this manuscript, we exploit the design path of transition-metal substitution in  $\text{Ca}_2\text{RuO}_4$  and demonstrate that it can reconfigure the spin-orbital magnon spectrum, leading to the emergence of one-magnon modes absent in the pristine material. Our Raman results, supported by theoretical modeling, reveal that hidden one-magnon excitations are activated by the breaking of mirror symmetry within the spin-orbital manifold. This effect, driven by local  $\text{RuO}_6$  octahedral distortions near the dopants, induces a mixing of even- and odd-parity states, thereby enabling the realization of mixed-parity magnon modes. Our results demonstrate that spin-orbit-lattice entanglement can be exploited to control and couple collective magnetic excitations, suggesting similar effects can be generally engineered via strain or lattice distortions.

*Experimental Results* – To investigate the impact of Mn substitution on the magnetic excitations of  $\text{Ca}_2\text{RuO}_4$ , we perform Raman spectroscopic measurements at cryogenic temperatures. Raman spectroscopy is a useful technique for directly probing magnetic excitations in ruthenates in the form of one- and multi-magnon modes [30, 54, 55], whose energies are directly related to the magnetic correlations between Ru ions.  $\text{Ca}_2\text{RuO}_4$  belongs to the orthorhombic space group  $\text{Pbca}$

(#61). For Raman measurements within the crystallographic  $ab$  plane, this space group yields excitations of  $A_g$  and of  $B_{1g}$  symmetry. In Fig. 1(a) we plot temperature dependent Raman data taken on  $\text{Ca}_2(\text{Ru},\text{Mn})\text{O}_4$  with 0%, 3%, 5%, and 10% Mn content. The outcomes at 0% are completely consistent with those reported in literature[30]. We can clearly identify  $T_N$  for each compound: at high temperatures ( $T > T_N$ ) there is an enhanced scattering background due to paramagnetic fluctuations. These fluctuations are quenched below  $T_N$ , resulting in a gapped background (this is most clearly seen for the sample with 0% Mn below  $\sim 60$  meV). Simultaneously, new one-magnon peaks, marked by arrows in each panel, emerge below  $T_N$ . For a better comparison of the evolution of phononic and magnetic excitations with increasing Mn content, we plot individual spectra of all four compounds obtained at a base temperature of  $T = 4$  K in Fig. 1(b). One-magnon modes are shaded, while partially overlapping phonons are marked by asterisks. The pure  $\text{Ca}_2\text{RuO}_4$  sample hosts a sharp and intense single one-magnon excitation at 12.5 meV (yellow-shaded), which is consistent with the previous report [30]. A partial substitution of Ru with 3% and 5% Mn yields two one-magnon branches with reduced intensity and increased linewidth (shaded green and red), while for a larger Mn content of 10% only a single, broadened and asymmetric magnon mode (yellow-shaded) can be resolved. The extracted parameters and energies are summarized in Table I, and one-magnon energy and intensity as a function of Mn content are plotted in Figs. 1(c) and (d). Consequently, even a small level of substitution shifts the one-magnon mode to higher energies and leads to the emergence of an additional magnetic peak, with a maximum intensity at an energy separation of approximately 1 meV. Further increases in Mn concentration continue to raise the magnon energy and result in

	Energy (meV)	FWHM (meV)	Intensity
0%	12.59	0.12	0.55
3%	13.54	0.43	0.29
	14.69	1.02	0.70
5%	13.84	0.43	0.23
	14.84	1.34	0.83
10%	16.06	1.34	0.84

TABLE I. Composition-dependent parameters energy, linewidth (FWHM), and intensity of the one-magnon modes measured at  $T = 4$  K.

a pronounced broadening of the spectral intensity, such that the two split peaks can no longer be distinguished. We further note that Mn–Ru substitution gives rise to additional low-energy magnetic excitations characterized by weak intensity and a broad continuum extending from approximately 5 to 8 meV. The associated spectral weight shows a slight increase with increasing Mn concentration. In addition to the low-energy magnetic modes, an extra phononic peak emerges near the phonon excitations at around 48 meV as a consequence of Mn substitution. By contrast, no significant modifications are observed in the higher-energy features within the 70–90 meV range.

Here, we concentrate on the one-magnon excitations in the cross-polarization channel, as they exhibit the most pronounced reconstruction upon Ru substitution.

*Magnetic model* – In  $\text{Ca}_2\text{RuO}_4$  the  $\text{Ru}^{4+}$  ions host four electrons in the  $t_{2g}$  shell, giving rise to local orbital and spin moments  $L = 1$  and  $S = 1$ . In the atomic limit, the intraionic SOC term  $\lambda \mathbf{L} \cdot \mathbf{S}$  stabilizes a nonmagnetic  $J = 0$  ground state, separated from the excited  $J = 1$  and  $J = 2$  multiplets. The competition between SOC and electron–lattice interactions — notably the flattening, rotation, and tilting of the  $\text{RuO}_6$  octahedra — drives the system away from the ideal  $J = 0$  configuration. Consequently, the low-energy manifold forms a quasi-triplet composed of the  $J = 0$  singlet and the two lowest components of the  $J = 1$  triplet [34]. These states define an effective local moment  $\mathbf{T}$  with total pseudospin  $T = 1$ , schematically illustrated in Fig. 2 (a) in terms of its spin-orbital composition.

Within this pseudospin basis, the nearest-neighbor exchange interactions in the  $\text{RuO}_2$  planes can be constructed by symmetry. For bonds along the  $x$  direction, the effective Hamiltonian reads

$$\mathcal{H}_x = \sum_{\langle i,j \rangle \parallel x} \left[ J_{xx} T_i^x T_j^x + J_{xy} T_i^y T_j^y + J_z T_i^z T_j^z \right], \quad (1)$$

where  $J_{xx}$ ,  $J_{xy}$ , and  $J_z$  are the anisotropic exchange couplings allowed by the orthorhombic symmetry. An analogous form  $\mathcal{H}_y$  applies for bonds along  $y$ , with  $J_{yy} = J_{xx}$  and  $J_{yx} = J_{xy}$ .

Local symmetry-lowering distortions, including the flattening, rotation and tilting of the  $\text{RuO}_6$  octahedra,

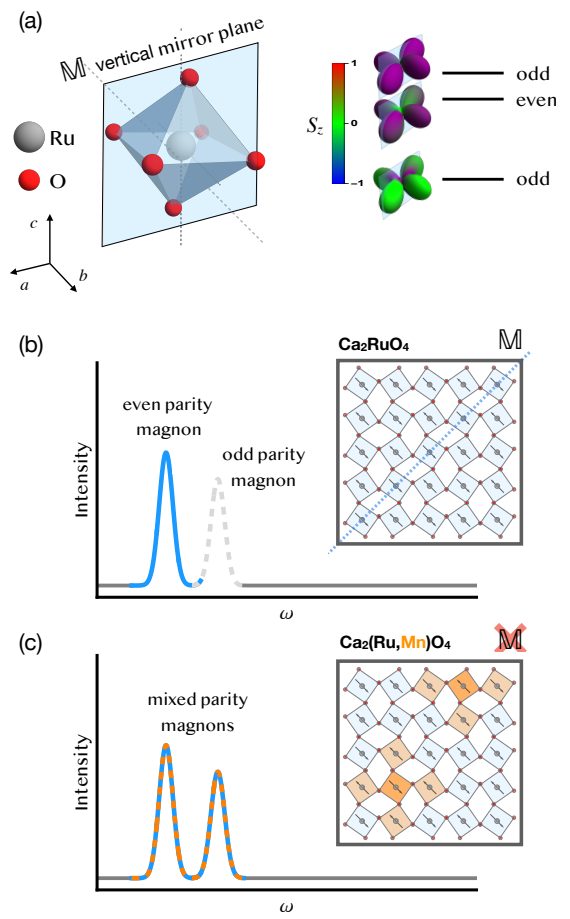


FIG. 2. (a) Schematic representation of the three lowest-lying local spin-orbital states stabilized by SOC and octahedral distortions in  $\text{Ca}_2\text{RuO}_4$ . The tilting of the  $\text{RuO}_6$  octahedra with respect to the  $b$  axis mixes the orbital characters and splits the multiplets into states of definite parity with respect to the diagonal vertical mirror (the vertical plane  $ac$  perpendicular to the  $b$  axis). The lowest state in energy has odd parity, while the higher-energy doublet consists of states with opposite parity, even/odd. The panel illustrates a representative case for distortions associated with a specific sign of the parameter  $\delta_c$  as related to the staggering of the octahedral rotations with respect to the  $c$ -axis; for the opposite sign, the parity of these two states is inverted. (b) and (c) schematically depict the evolution of the magnon spectrum for the antiferromagnetic state from the undoped to the Mn-doped (orange) configuration with the substitution being a source of diagonal vertical mirror (M) symmetry breaking. The breaking of the vertical mirror activates a one-magnon mode in the cross polarization channel that is silent in the  $\text{Ca}_2\text{RuO}_4$  compound (c). Here, we focus on the excitations of the Ru magnetic moments, with the oxygen degrees of freedom projected out. This enables the application of a mirror transformation to the Ru lattice and the associated spin configuration, as schematically illustrated in panel (b).

introduce additional on-site staggered contributions (Fig. 2 b) [56]

$$\mathcal{H}_{\text{loc}} = E_T \sum_j (T_j^z)^2 + \delta_c \sum_j (-1)^j (T_j^x T_j^y + T_j^y T_j^x) + \delta_b \sum_j (-1)^j [T_j^z (T_j^x + T_j^y) + (T_j^x + T_j^y) T_j^z], \quad (2)$$

where  $E_T$  is the single-ion anisotropy due to axial compression along the  $c$  axis, and  $\delta_c$ ,  $\delta_b$  represent the anisotropy terms associated with staggered octahedral rotations and tilts about the  $c$  and  $b$  axes, respectively. X-ray studies on Mn-doped  $\text{Ca}_2\text{RuO}_4$  report local structural relaxations around the impurity sites, which in turn lead to concomitant modifications of the magnetic order [41]. In our model, the effects of impurities at dilute concentrations mainly affect the local crystal field environment. Specifically, since Mn enters with a  $d^3$  non-Jahn Teller configuration, the substitution tends to symmetrize the octahedral Ru-O bonds by reducing the tetragonal energy splitting  $\Delta_T$ . Hence, we effectively assume that the Mn dopant amplifies the amplitude of the  $E_T$  term, as it scales as  $\lambda^2/\Delta_T$ , [14].

We now describe the symmetry aspects of the low energy magnon modes that are crucial to account for their reconstruction upon Mn substitution. The low-energy spin-orbital states of the  $t_{2g}$  manifold ( $L = 1, S = 1$ ) couple anisotropically to the lattice via octahedral compression, rotation about the  $c$  axis, and tilting relative to the  $b$  axis. These states can be classified by their parity under the vertical mirror operation  $\mathcal{M}_b$  (Fig. 2(a)). Specifically, the ground-state singlet (adiabatically connected to the  $J = 0$  state) is  $\mathcal{M}_b$ -odd, whereas the excited doublet ( $J = 1$  subspace) comprises states of opposite parity. In the effective magnetic exchange model, these map to the  $T = 1$  states  $\{|\tilde{1}\rangle, |\tilde{0}\rangle, |-\tilde{1}\rangle\}$ , which diagonalize the local Hamiltonian of Eq. 2 and satisfy the aforementioned symmetry constraints, as explicitly shown in the Supplemental Material.

In pristine  $\text{Ca}_2\text{RuO}_4$ , the vertical mirror symmetry is globally preserved within the lattice, and the corresponding mirror-parity quantum number governs the selection rules for magnetic excitations and their coupling to external probes, including Raman scattering. In the full Hamiltonian  $\mathcal{H}$ , this symmetry is properly defined by the operator  $\mathbb{M} \equiv M \otimes \prod_j \mathcal{M}_b^j$ , which combines the local action  $\mathcal{M}_b^j$  on site  $j$  with the spatial mirror  $M$  mapping the coordinates as  $(x, y) \xrightarrow{M} (-y, -x)$ . Consequently, two symmetry-distinct one-magnon branches,  $|\psi_1\rangle$  and  $|\psi_2\rangle$ , are expected; these branches are even and odd, respectively, under the global mirror operation, such that  $\mathbb{M}|\psi_1\rangle = |\psi_1\rangle$  and  $\mathbb{M}|\psi_2\rangle = -|\psi_2\rangle$ . An explicit demonstration of this symmetry based construction is provided in the Supplemental Material. Assuming the local terms dominate, we perform a perturbative expansion in the exchange coupling and derive the energies of the two

magnons relative to the ground-state energy  $E_0$ , which at leading order in  $\delta_b$  and  $\delta_c$  are expressed as

$$E_1 - E_0 = E_T - 2(J_{xx} + J_{xy}) - \frac{\delta_c^2}{4(J_{xx} + J_{xy})} \frac{2\delta_b^2}{E_T} + \left(2 - \frac{E_T}{J_{xx} + J_{xy}}\right) \frac{\delta_c^2 \delta_b^2}{E_T^3}, \quad (3)$$

$$E_2 - E_0 = E_T - 2(J_{xx} + J_{xy}) - \frac{\delta_c^2}{4(J_{xx} + J_{xy})} \frac{4\delta_b^2}{E_T} + \left(4 + \frac{E_T}{J_{xx} + J_{xy}}\right) \frac{\delta_c^2 \delta_b^2}{E_T^3}. \quad (4)$$

These expressions for the one-magnon modes naturally account for the energy shift induced by an increase in the anisotropy magnetic energy  $E_T$ , as well as for the emergence of split magnon modes, whose energy separation depends on both the magnitude of the octahedral distortions and the strength of the magnetic exchange.

*Model calculations and connection with Raman experiments* – To describe the Raman spectra, we adopt the Loudon–Fleury (LF) framework [57], with the Raman scattering operator being defined as

$$R \propto \sum_{\langle i, j \rangle} (\epsilon_{\text{in}} \cdot \mathbf{r}_{ij}) (\epsilon_{\text{out}} \cdot \mathbf{r}_{ij}) \mathcal{H}_{ij}, \quad (5)$$

where  $\epsilon_{\text{in}}$  and  $\epsilon_{\text{out}}$  are the incoming and outgoing polarization vectors, and  $\mathcal{H}_{ij}$  denotes the Hamiltonian on bond  $\langle i, j \rangle$ , which includes both exchange interactions  $\mathcal{H}_x$  and  $\mathcal{H}_y$  [57].

When the light polarizations are confined to the  $ab$  plane,  $\epsilon_{\text{in}(\text{out})}$  can be specified by their in-plane angles with respect to the crystallographic  $a$  axis. In the  $B_{1g}$  geometry adopted in the experiments, the Raman operator reduces to

$$R_{B_{1g}} = \sum_{\langle i, j \rangle_x} \mathcal{H}_{ij} - \sum_{\langle i, j \rangle_y} \mathcal{H}_{ij}, \quad (6)$$

In pure  $\text{Ca}_2\text{RuO}_4$ , only a one-magnon branch is observed in Raman scattering within the  $B_{1g}$  symmetry channel, as schematically shown in Fig. 2 (b). This selective visibility is determined by two factors: (i) the symmetry of the Raman tensor, which transforms as odd under the mirror operation  $\mathbb{M}$ , and (ii) the symmetry of the magnetic exchange Hamiltonian, which, in contrast, is even under  $\mathbb{M}$ . As a result, only the first magnon branch, whose mirror parity is compatible with the Raman tensor (i.e., even) can couple to light in the  $B_{1g}$  channel. The second branch, which is odd under  $\mathbb{M}$ , remains Raman inactive in this symmetry channel and allowed in the  $A_g$  symmetry. However, the experimental observations here and in the literature [30] indicate that this

magnetic mode is fully obscured in the  $A_g$  channel due to the spin-phonon coupling. This is commonly observed in magnetic materials because fully symmetric magnetic excitations hybridize strongly with  $A_g$  phonons, leading to pronounced screening and damping of the spectral weight. The appearance of an additional  $B_{1g}$  Raman-active magnon in Mn-substituted samples thus signals a lowering of the local symmetry and the onset of mixed mirror-parity character in the magnetic excitations.

The substitution of Ru by Mn in  $\text{Ca}_2\text{Ru}_{1-x}\text{Mn}_x\text{O}_4$  acts as a local symmetry-breaking perturbation. The Mn ions locally relax the octahedral compression around the impurity sites and thereby disrupt the global mirror symmetry  $M$  of the crystal lattice. This perturbation modifies both the crystal-field environment and the superexchange pathways, effectively mixing magnon states of different mirror parity. As a result of Mn substitution, the mirror operation  $M$  ceases to be an exact symmetry of the magnetic lattice. Consequently, the one-magnon excitations can no longer be classified by a well-defined mirror parity. The breaking of this symmetry lifts the selection rules that protect certain excitations, thereby activating mixed-parity one-magnon modes that are otherwise hidden in the high-symmetry phase (Fig. 2 (c)).

To substantiate these symmetry-based results we perform exact-diagonalization (ED) calculations of the Raman spectrum on finite clusters, with various distributions of Mn impurities. The calculations are carried out using the full pseudospin Hamiltonian  $\mathcal{H} = \mathcal{H}_{loc} + \mathcal{H}_x + \mathcal{H}_y$ . The Raman operator  $R_{B_{1g}}$  is implemented according to Eq. (6), and the Raman intensity spectral function is given by

$$I(\omega) = \sum_n |\langle n | R_{B_{1g}} | 0 \rangle|^2 \delta(\omega - E_n + E_0). \quad (7)$$

In Fig. 3, we present representative cases for both (a) the undoped and single-impurity configurations and (b) the two-impurity configurations. Our focus is on the lowest-energy magnon mode, which is most relevant for the experimental observations. In the undoped case, a single one-magnon mode can be reproduced at approximately 12 meV assuming the following model parameters,  $J_{xx} = 5.2$  meV,  $J_{xy} = 3.1$  meV,  $J_z = 2$  meV,  $E_T = 30$  meV which are compatible with the  $\text{Ca}_2\text{RuO}_4$  magnetic properties [14, 33].

The introduction of an impurity breaks the vertical mirror symmetry by inducing a short-range anisotropic structural distortion around the impurity, consistent with the orthorhombicity of the crystal lattice. Depending on the magnitude of this local structural change, the strength of the mirror-symmetry breaking can be tuned, resulting in a shift of the emerging double-peak magnon structure to higher energies (Fig. 3(a)).

Increasing the number of impurities, e.g. from one to two as in Fig. 3(b), modulates the relative intensity of the two peaks and redistributes the magnon spectral weight,

depending on the positions of the impurities relative to the magnetic sublattice and the gradient profile of the structural potential. When averaging over different impurity configurations, these effects produce a shift in the magnon energies and a finite broadening of the Raman spectral intensity. The resulting outcomes can fairly reproduce the qualitative changes of the Raman spectra observed in the experiments as a function of the Mn concentration.

*Conclusions* – We have shown that partial  $\text{Ru} \rightarrow \text{Mn}$  substitution in  $\text{Ca}_2\text{RuO}_4$  reconstructs the magnon spectrum and activates one-magnon excitations that are hidden in the undoped material. This effect arises from local mirror-symmetry breaking of the spin-orbital configuration, induced by structural distortions of the  $\text{RuO}_6$  octahedra near the dopant, and demonstrates the critical role of spin-orbit-lattice entanglement in shaping collective magnetic excitations. Our findings highlight that spin-orbital magnons are highly sensitive to local structural and electronic perturbations, providing a pathway to control magnetic dynamics beyond conventional spin-only physics. More broadly, the mechanism uncovered here suggests that hidden magnons could be selectively accessed through dopants, strain, or other lattice distortions in a wide range of spin-orbit correlated materials, opening opportunities to engineer magnonic spectra and design novel functionalities in quantum and spintronic devices.

M.C., F.F., R.F., A.G. and A.V. acknowledge partial support by the Italian Ministry of Foreign Affairs and International Cooperation, grant KR23GR06. F.F. and F.G. acknowledge support from the Italian Ministry of University and Research (MUR) under the National Recovery and Resilience Plan (NRRP), Call PRIN 2022, funded by the European Union - NextGenerationEU, Mission 4, Component 2, Grant No. 2022TWZ9NR (STIMO)-CUP B53D23004560006. M.C. and A.V. acknowledge support by Italian MUR PRIN 2022 under the Grant No. 2022LP5K7 (BEAT). M.C. and F.F. acknowledge support from PNRR MUR project PE0000023-NQSTI. W.B. acknowledges support by Narodowe Centrum Nauki (NCN, National Science Centre, Poland) Project No. 2021/43/B/ST3/02166 and by the Foundation for Polish Science project MagTop no. FENG.02.01IP.05-0028/23 co-financed by the European Union from the funds of Priority 2 of the European Funds for a Smart Economy Program 2021–2027 (FENG). D.W. acknowledges support from the Institute of Applied Physics of Seoul National University.

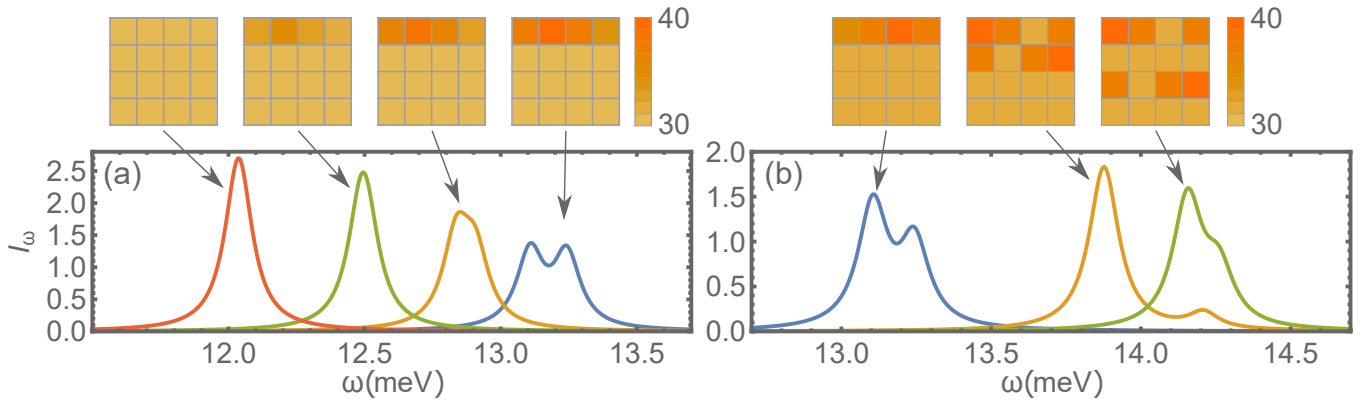


FIG. 3. Raman spectral function evaluated for a  $4 \times 4$  cluster with periodic boundary conditions and in the presence of inhomogeneous anisotropic magnetic energy  $E_T$  nearby the substituted site (corresponding to the darkest orange square in the schematic cluster). The parameters of the model are  $J_{xx} = 5.2$ ,  $J_{xy} = 3.1$ ,  $J_z = 2$ ,  $E_T = 30$  (in units of meV) at host sites. At the impurity sites the anisotropic magnetic energy  $E_T$  is modified to acquire the value  $E_T = 40$  and is also varied at the neighboring sites of the impurity, as illustrated by the contour map. For clarity we employ Lorentzian distributions for the spectral function with broadening factor  $\eta = 0.06$  meV.

[2] G. Khaliullin, Orbital order and fluctuations in Mott insulators, *Progress of Theoretical Physics Supplement* **160**, 155 (2005), <https://academic.oup.com/ptps/article-pdf/doi/10.1143/PTPS.160.155/5162453/160-155.pdf>.

[3] G. Cao and P. Schlottmann, The challenge of spin-orbit-tuned ground states in iridates: a key issues review, *Reports on Progress in Physics* **81**, 042502 (2018).

[4] T. Takayama, J. Chaloupka, A. Smerald, G. Khaliullin, and H. Takagi, Spin-orbit-entangled electronic phases in 4d and 5d transition-metal compounds, *Journal of the Physical Society of Japan* **90**, 062001 (2021), <https://doi.org/10.7566/JPSJ.90.062001>.

[5] D. Pesin and L. Balents, Mott physics and band topology in materials with strong spin-orbit interaction, *Nature Physics* **6**, 376 (2010).

[6] C. S. Alexander, G. Cao, V. Dobrosavljevic, S. McCall, J. E. Crow, E. Lochner, and R. P. Guertin, Destruction of the Mott insulating ground state of  $\text{Ca}_2\text{RuO}_4$  by a structural transition, *Phys. Rev. B* **60**, R8422 (1999).

[7] S. Nakatsuji and Y. Maeno, Quasi-two-dimensional Mott transition system  $\text{Ca}_{2-x}\text{Sr}_x\text{RuO}_4$ , *Phys. Rev. Lett.* **84**, 2666 (2000).

[8] S. Ricco, M. Kim, A. Tamai, S. McKeown Walker, F. Y. Bruno, I. Cucchi, E. Cappelli, C. Besnard, T. K. Kim, P. Dudin, M. Hoesch, M. J. Gutmann, A. Georges, R. S. Perry, and F. Baumberger, In situ strain tuning of the metal-insulator-transition of  $\text{Ca}_2\text{RuO}_4$  in angle-resolved photoemission experiments, *Nature Communications* **9**, 4535 (2018).

[9] O. Friedt, M. Braden, G. André, P. Adelmann, S. Nakatsuji, and Y. Maeno, Structural and magnetic aspects of the metal-insulator transition in  $\text{Ca}_{2-x}\text{Sr}_x\text{RuO}_4$ , *Phys. Rev. B* **63**, 174432 (2001).

[10] G. Cuono and C. Autieri, Mott insulator  $\text{Ca}_2\text{RuO}_4$  under external electric field, *Materials* **15**, 10.3390/ma15196657 (2022).

[11] N. Gauquelin, F. Forte, D. Jannis, R. Fittipaldi, C. Autieri, G. Cuono, V. Granata, M. Lettieri, C. Noce, F. Miletto-Granozio, A. Vecchione, J. Verbeeck, and M. Cuoco, Pattern formation by electric-field quench in a Mott crystal, *Nano Letters* **23**, 7782 (2023).

[12] G. Cuono, F. Forte, A. Romano, and C. Noce, Emerging new phases in correlated mott insulator  $\text{Ca}_2\text{RuO}_4$ , *Journal of Physics: Condensed Matter* **37**, 053002 (2024).

[13] D. Sutter, C. Fatuzzo, S. Moser, M. Kim, R. Fittipaldi, A. Vecchione, V. Granata, Y. Sassa, F. Cossalter, G. Gatti, M. Grioni, H. M. Rønnow, N. C. Plumb, C. E. Matt, M. Shi, M. Hoesch, T. K. Kim, T. R. Chang, H. T. Jeng, C. Jozwiak, A. Bostwick, E. Rotenberg, A. Georges, T. Neupert, and J. Chang, Hallmarks of Hund's coupling in the Mott insulator  $\text{Ca}_2\text{RuO}_4$ , *Nat. Comm.* **8**, 15176 (2017).

[14] L. Das, F. Forte, R. Fittipaldi, C. G. Fatuzzo, V. Granata, O. Ivashko, M. Horio, F. Schindler, M. Dantz, Y. Tseng, D. E. McNally, H. M. Rønnow, W. Wan, N. B. Christensen, J. Pelliciari, P. Olalde-Velasco, N. Kikugawa, T. Neupert, A. Vecchione, T. Schmitt, M. Cuoco, and J. Chang, Spin-Orbital Excitations in  $\text{Ca}_2\text{RuO}_4$  Revealed by Resonant Inelastic X-Ray Scattering, *Phys. Rev. X* **8**, 011048 (2018).

[15] F. Nakamura, H. Ogura, T. Sakami, and T. Suzuki, Unique itinerant ferromagnetism in 4d electron system  $\text{Ca}_2\text{RuO}_4$ , *JPS Conf. Proc.* **38**, 011128 (2023).

[16] A. Jain, M. Krautloher, J. Porras, G. H. Ryu, D. P. Chen, D. L. Abernathy, J. T. Park, A. Ivanov, J. Chaloupka, G. Khaliullin, B. Keimer, and B. J. Kim, Higgs mode and its decay in a two-dimensional antiferromagnet, *Nat. Phys.* **13**, 633 (2017).

[17] W. Brzezicki, F. Forte, C. Noce, M. Cuoco, and A. M. Oleś, Spin-orbital mechanisms for negative thermal expansion in  $\text{Ca}_2\text{RuO}_4$ , *Phys. Rev. B* **107**, 104403 (2023).

[18] F. Nakamura, M. Sakaki, Y. Yamanaka, S. Tamaru, T. Suzuki, and Y. Maeno, Electric-field-induced metal maintained by current of the Mott insulator  $\text{Ca}_2\text{RuO}_4$ , *Scientific Reports* **3**, 2536 (2013).

[19] I. Terasaki, I. Sano, K. Toda, S. Kawasaki, A. Nakano, H. Taniguchi, H. J. Cho, H. Ohta, and F. Nakamura, Non-equilibrium steady state in the Mott insulator  $\text{Ca}_2\text{RuO}_4$ , *Journal of the Physical Society of Japan* **89**,

093707 (2020).

[20] J. Bertinshaw, N. Gurung, P. Jorba, H. Liu, M. Schmid, D. T. Mantadakis, M. Daghofer, M. Krautloher, A. Jain, G. H. Ryu, O. Fabelo, P. Hansmann, G. Khaliullin, C. Pfleiderer, B. Keimer, and B. J. Kim, Unique crystal structure of  $\text{Ca}_2\text{RuO}_4$  in the current stabilized semimetallic state, *Phys. Rev. Lett.* **123**, 137204 (2019).

[21] C. Cirillo, V. Granata, G. Avallone, R. Fittipaldi, C. Attanasio, A. Avella, and A. Vecchione, Emergence of a metallic metastable phase induced by electrical current in  $\text{Ca}_2\text{RuO}_4$ , *Phys. Rev. B* **100**, 235142 (2019).

[22] D. Curcio, C. E. Sanders, A. Chikina, H. E. Lund, M. Bianchi, V. Granata, M. Cannavacciuolo, G. Cuono, C. Autieri, F. Forte, G. Avallone, A. Romano, M. Cuoco, P. Dudin, J. Avila, C. Polley, T. Balasubramanian, R. Fittipaldi, A. Vecchione, and P. Hofmann, Current-driven insulator-to-metal transition without Mott breakdown in  $\text{Ca}_2\text{RuO}_4$ , *Phys. Rev. B* **108**, L161105 (2023).

[23] C. T. Suen, I. Marković, M. Zonno, N. Heinsdorf, S. Zhdanovich, N. H. Jo, M. Schmid, P. Hansmann, P. Puphal, K. Fürsich, S. Smit, C. Au-Yeung, V. Zimermann, B. Zwartsenberg, M. Krautloher, I. S. Elfimov, R. Koch, S. Gorovikov, C. Jozwiak, A. Bostwick, M. Franz, E. Rotenberg, B. Keimer, and A. Damascelli, Electronic response of a Mott insulator at a current-induced insulator-to-metal transition, *Nature Physics* **20**, 1757 (2024).

[24] J. Zhang, A. S. McLeod, Q. Han, X. Chen, H. A. Bechtel, Z. Yao, S. N. Gilbert Corder, T. Ciavatti, T. H. Tao, M. Aronson, G. L. Carr, M. C. Martin, C. Sow, S. Yonezawa, F. Nakamura, I. Terasaki, D. N. Basov, A. J. Millis, Y. Maeno, and M. Liu, Nano-resolved current-induced insulator-metal transition in the Mott insulator  $\text{Ca}_2\text{RuO}_4$ , *Phys. Rev. X* **9**, 011032 (2019).

[25] K. Fürsich, J. Bertinshaw, P. Butler, M. Krautloher, M. Minola, and B. Keimer, Raman scattering from current-stabilized nonequilibrium phases in  $\text{Ca}_2\text{RuO}_4$ , *Phys. Rev. B* **100**, 081101 (2019).

[26] V. K. Bhartiya, R. Hartmann, F. Forte, F. Gabriele, T. Kim, G. Cuono, C. Autieri, S. Fan, K. Kisslinger, F. Camino, M. Lettieri, R. Fittipaldi, C. Mazzoli, D. N. Basov, J. Pelliciari, A. D. Bernardo, A. Vecchione, M. Cuoco, and V. Bisogni, Evidence of electronic states driving current-induced insulator-to-metal transition (2025), arXiv:2504.17871 [cond-mat.str-el].

[27] S. Nakatsuji, S.-i. Ikeda, and Y. Maeno,  $\text{Ca}_2\text{RuO}_4$ : New Mott insulators of layered ruthenate, *Journal of the Physical Society of Japan* **66**, 1868 (1997).

[28] G. Cao, S. McCall, M. Shepard, J. E. Crow, and R. P. Guertin, Magnetic and transport properties of single-crystal  $\text{Ca}_2\text{RuO}_4$ : relationship to superconducting  $\text{Sr}_2\text{RuO}_4$ , *Phys. Rev. B* **56**, R2916 (1997).

[29] M. Braden, G. André, S. Nakatsuji, and Y. Maeno, Crystal and magnetic structure of  $\text{Ca}_2\text{RuO}_4$ : Magnetoelastic coupling and the metal-insulator transition, *Phys. Rev. B* **58**, 847 (1998).

[30] S.-M. Souliou, J. Chaloupka, G. Khaliullin, G. Ryu, A. Jain, B. J. Kim, M. Le Tacon, and B. Keimer, Raman scattering from Higgs mode oscillations in the two-dimensional antiferromagnet  $\text{Ca}_2\text{RuO}_4$ , *Phys. Rev. Lett.* **119**, 067201 (2017).

[31] D. G. Porter, V. Granata, F. Forte, S. Di Matteo, M. Cuoco, R. Fittipaldi, A. Vecchione, and A. Bombardi, Magnetic anisotropy and orbital ordering in  $\text{Ca}_2\text{RuO}_4$ , *Phys. Rev. B* **98**, 125142 (2018).

[32] C. G. Fatuzzo, M. Dantz, S. Fatale, P. Olalde-Velasco, N. E. Shaik, B. Dalla Piazza, S. Toth, J. Pelliciari, R. Fittipaldi, A. Vecchione, N. Kikugawa, J. S. Brooks, H. M. Rønnow, M. Grioni, C. Rüegg, T. Schmitt, and J. Chang, Spin-orbit-induced orbital excitations in  $\text{Sr}_2\text{RuO}_4$  and  $\text{Ca}_2\text{RuO}_4$ : A resonant inelastic x-ray scattering study, *Phys. Rev. B* **91**, 155104 (2015).

[33] H. Gretarsson, H. Suzuki, H. Kim, K. Ueda, M. Krautloher, B. J. Kim, H. Yavaş, G. Khaliullin, and B. Keimer, Observation of spin-orbit excitations and Hund's multiplets in  $\text{Ca}_2\text{RuO}_4$ , *Phys. Rev. B* **100**, 045123 (2019).

[34] G. Khaliullin, Excitonic magnetism in van Vleck-type  $d^4$  mott insulators, *Phys. Rev. Lett.* **111**, 197201 (2013).

[35] F. Forte, M. Cuoco, and C. Noce, Field-induced orbital patterns in ferromagnetic layered ruthenates, *Phys. Rev. B* **82**, 155104 (2010).

[36] T. Feldmaier, P. Strobel, M. Schmid, P. Hansmann, and M. Daghofer, Excitonic magnetism at the intersection of spin-orbit coupling and crystal-field splitting, *Phys. Rev. Res.* **2**, 033201 (2020).

[37] P. M. Sarte, C. Stock, B. R. Ortiz, K. H. Hong, and S. D. Wilson, Van Vleck excitons in  $\text{Ca}_2\text{RuO}_4$ , *Phys. Rev. B* **102**, 245119 (2020).

[38] P. Steffens, O. Friedt, P. Alireza, W. G. Marshall, W. Schmidt, F. Nakamura, S. Nakatsuji, Y. Maeno, R. Lengsdorf, M. M. Abd-Elmeguid, and M. Braden, High-pressure diffraction studies on  $\text{Ca}_2\text{RuO}_4$ , *Phys. Rev. B* **72**, 094104 (2005).

[39] T. F. Qi, O. B. Korneta, S. Parkin, L. E. De Long, P. Schlottmann, and G. Cao, Negative volume thermal expansion via orbital and magnetic orders in  $\text{Ca}_2\text{Ru}_{1-x}\text{Cr}_x\text{O}_4$  ( $0 < x < 0.13$ ), *Phys. Rev. Lett.* **105**, 177203 (2010).

[40] S. Chi, F. Ye, G. Cao, H. Cao, and J. A. Fernandez-Baca, Competition of three-dimensional magnetic phases in  $\text{Ca}_2\text{Ru}_{1-x}\text{Fe}_x\text{O}_4$ : A structural perspective, *Phys. Rev. B* **102**, 014452 (2020).

[41] D. G. Porter, F. Forte, V. Granata, M. Cannavacciuolo, R. Fittipaldi, M. Cuoco, A. Bombardi, and A. Vecchione, Guiding antiferromagnetic transitions in  $\text{Ca}_2\text{RuO}_4$ , *Scientific Reports* **12**, 10957 (2022).

[42] D. Tian, L. Miao, L. Si, N. J. Schreiber, S. Shen, J. Zhang, X. Shu, X. Wang, H. P. Nair, J. P. Ruf, D. G. Schlom, K. M. Shen, and P. Yu, Tuning the electronic and magnetic states of  $\text{Ca}_2\text{RuO}_4$  with proton evolution, *Phys. Rev. Mater.* **8**, 074408 (2024).

[43] S. Kunkemöller, E. Komleva, S. V. Strelnsov, S. Hoffmann, D. I. Khomskii, P. Steffens, Y. Sidis, K. Schmalzl, and M. Braden, Magnon dispersion in  $\text{Ca}_2\text{Ru}_{1-x}\text{Ti}_x\text{O}_4$ : Impact of spin-orbit coupling and oxygen moments, *Phys. Rev. B* **95**, 214408 (2017).

[44] D. Pincini, S. Boscaglia, R. Perry, M. J. Gutmann, S. Riccò, L. S. I. Veiga, C. D. Dashwood, S. P. Collins, G. Nisbet, A. Bombardi, D. G. Porter, F. Baumberger, A. T. Boothroyd, and D. F. McMorrow, Persistence of antiferromagnetic order upon La substitution in the  $4d^4$  Mott insulator  $\text{Ca}_2\text{RuO}_4$ , *Phys. Rev. B* **98**, 014429 (2018).

[45] W. Brzezicki, A. M. Oleś, and M. Cuoco, Spin-orbital order modified by orbital dilution in transition-metal oxides: From spin defects to frustrated spins polarizing host orbitals, *Phys. Rev. X* **5**, 011037 (2015).

[46] W. Brzezicki, F. Forte, C. Noce, M. Cuoco, and A. M.

Oleś, Tuning crystal field potential by orbital dilution in strongly correlated  $d^4$  oxides, *Journal of Superconductivity and Novel Magnetism* **33**, 2375 (2020).

[47] W.-H. Li, C. H. Perry, J. B. Sokoloff, V. Wagner, M. E. Chen, and G. Shirane, Polarized neutron studies of forbidden magnons in the two-dimensional ferromagnet  $K_2CuF_4$ , *Phys. Rev. B* **35**, 1891 (1987).

[48] A. Etesamirad, J. Kharlan, R. Rodriguez, I. Barsukov, and R. Verba, Controlling selection rules for magnon scattering in nanomagnets by spatial symmetry breaking, *Phys. Rev. Appl.* **19**, 044087 (2023).

[49] T. W. J. Metzger, K. A. Grishunin, C. Reinhoffer, R. M. Dubrovin, A. Arshad, I. Ilyakov, T. V. A. G. de Oliveira, A. Ponomaryov, J.-C. Deinert, S. Kovalev, R. V. Pisarev, M. I. Katsnelson, B. A. Ivanov, P. H. M. van Loosdrecht, A. V. Kimel, and E. A. Mashkovich, Magnon-phonon Fermi resonance in antiferromagnetic  $CoF_2$ , *Nature Communications* **15**, 5472 (2024).

[50] G. Gitgeatpong, Y. Zhao, P. Piyawongwatthana, Y. Qiu, L. W. Harriger, N. P. Butch, T. J. Sato, and K. Matan, Nonreciprocal magnons and symmetry-breaking in the noncentrosymmetric antiferromagnet, *Phys. Rev. Lett.* **119**, 047201 (2017).

[51] S. M. Winter, K. Riedl, P. A. Maksimov, A. L. Chernyshev, A. Honecker, and R. Valentí, Breakdown of magnons in a strongly spin-orbital coupled magnet, *Nature Communications* **8**, 1152 (2017).

[52] H.-H. Kim, K. Ueda, S. Nakata, P. Wochner, A. Mackenzie, C. Hicks, G. Khaliullin, H. Liu, B. Keimer, and M. Minola, Giant stress response of terahertz magnons in a spin-orbit Mott insulator, *Nature Communications* **13**, 6674 (2022).

[53] X. Chen, Y. Liu, P. Liu, Y. Yu, J. Ren, J. Li, A. Zhang, and Q. Liu, Unconventional magnons in collinear magnets dictated by spin space groups, *Nature* **640**, 349 (2025).

[54] J. H. Lee, D. Wulferding, J. Kim, D. Song, S. R. Park, and C. Kim, Linear scaling relationship of Néel temperature and dominant magnons in pyrochlore ruthenates, *Phys. Rev. B* **108**, 054443 (2023).

[55] D. Wulferding, J. Kim, M. K. Kim, Y. Yang, J. H. Lee, D. Song, D. Oh, H.-S. Kim, L. E. Chern, Y. B. Kim, M. Noh, H. Choi, S. Choi, N. B. Perkins, C. Kim, and S. R. Park, Collective magnetic Higgs excitation in a pyrochlore ruthenate, *npj Quantum Materials* **8**, 40 (2023).

[56] H. Liu and G. Khaliullin, Pseudo-Jahn-Teller effect and magnetoelastic coupling in spin-orbit Mott insulators, *Phys. Rev. Lett.* **122**, 057203 (2019).

[57] P. A. Fleury and R. Loudon, Scattering of light by one- and two-magnon excitations, *Phys. Rev.* **166**, 514 (1968).